Journal of Cultural Heritage 67 (2024) 336–351

Contents lists available at ScienceDirect

Journal of Cultural Heritage

journal homepage: www.elsevier.com/locate/culher

Original article

Automatic analysis of pottery sherds based on structure from motion scanning: The case of the Phoenician carinated-shoulder amphorae from Tell el-Burak (Lebanon)

Luca Di Angelo[a,b,*], Aaron Schmitt[c], Michael Rummel[c], Paolo Di Stefano[a,b]

[a] Department of Industrial and Information Engineering, and of Economics, University of L'Aquila, via G. Gronchi 18, 67100 L'Aquila, Italy
[b] Heritechne, University of L'Aquila, Piazzale Pontieri 1, 67040 Monteluco di Roio, AQ, Italy
[c] Center for Ancient Studies - Institute for Pre- and Protohistory and Near Eastern Archeology - University of Heidelberg, Sandgasse 7, 69117, Heidelberg, Germany

ARTICLE INFO

Article history:
Received 18 May 2023
Accepted 16 March 2024

Keywords:
3D archeology
Automatic feature recognition
Structure from motion
Pottery
Phoenician amphorae
Hierarchical rims clusterization

ABSTRACT

Over the last few years, significant interest has been addressed in developing computer-based methods to document and analyze fragments of ceramics sherds in archaeology. This is because traditional manual processes do not allow for an objective, repeatable, and reproducible analysis of the large quantities of material needed to fully understand and explain human practices in various cultural contexts, such as the economy, daily life, and the material expression of religious beliefs.

In that context, this paper proposes a fully digital methodology resulting from the constitution of an international research group coming from different scientific backgrounds: archaeologists with specific skills and experience in fast 3D geometry acquisition methods and researchers who developed and published the only available computer-based process for recognizing the geometric and morphological sherds features analyzed by archaeologists. The proposed methodology consists of two main parts: 1. 3D acquisition of sherds with the construction of the discrete 3D manifold model based on the Structure for Motion technologies; 2. recognition, segmentation, and dimensional characterization of morphological and geometrical features based on the codification and algorithmic implementation of the knowledge used by the archeologists in the traditional method. The method was applied to analyze a set of 133 sherds excavated at Tell el-Burak (Lebanon) to obtain, through the analysis of the namely Phoenician carinated-shoulder amphorae, new insights into the economic organization of the Phoenician homeland. The method demonstrated the potential for objectively, repeatedly, and reproducibly analyzing large quantities of sherds. Furthermore, it allowed studying sherds by generating new high-level knowledge from those acquired from 3D models; in particular, this paper introduces new morphological features that help the archaeologist classify fragments from an analysis of the rim's shape.

© 2024 The Author(s). Published by Elsevier Masson SAS on behalf of Consiglio Nazionale delle Ricerche (CNR).
This is an open access article under the CC BY-NC-ND license (http://creativecommons.org/licenses/by-nc-nd/4.0/)

Introduction

According to the recommendations of the "UNESCO, ICCROM, ICOMOS (1994)" (Nara Document on Authenticity, article 13. http://www.international.icomos.org/charters/narae.html), the preservation of the authenticity and integrity of archaeological excavations and finds is a necessary objective of the cultural heritage (CH). These objectives must be achieved in all activities attributable to CH:

- Archaeological excavation;
- Archaeological research;
- Archive management;
- Conservation;
- Exhibition;
- Utilization of cultural heritage.

Despite the scientific community's efforts, these goals still need to be satisfactorily achieved. This condition is common to all artifacts, including ceramics. Ceramic containers were an essential part of various human practices before the inception of polymers. Pottery, i. e. mainly fragments of burnt clay vessels, are the most

* Corresponding author.
E-mail address: luca.diangelo@univaq.it (L. Di Angelo).

https://doi.org/10.1016/j.culher.2024.03.012
1296-2074/© 2024 The Author(s). Published by Elsevier Masson SAS on behalf of Consiglio Nazionale delle Ricerche (CNR). This is an open access article under the CC BY-NC-ND license (http://creativecommons.org/licenses/by-nc-nd/4.0/)

abundant finds during most excavations. Due to their omnipresence and abundance in archaeological contexts, the study of ceramics can inform many research questions addressing human behavior and decision-making in the past. However, documenting and analyzing the enormous quantity of pottery produced during excavations is still a significant challenge in archaeology [1]. In a previous paper [2], the authors demonstrated that the traditional method for shape and dimensional characterization, based on the graphical representation of sherds, is neither reproducible nor repeatable, even for “indicative” or “diagnostic” ones.

For this purpose, over the last three decades, the development of digital methods for the documentation of archaeological artifacts has been given much attention [3–6]. Among all these approaches, the only one capable of recognizing some of the significant geometric and morphological features analyzed by archaeologists is the one proposed by the research group of the University of L’Aquila and published in [2,7,8]. The segmentation method is based on the differential geometrical properties and topological invariants analyses. The published methods, starting from the discretized models of the sherds, automatically segment axially-symmetric features (the rim, internal and external wall, and base) and non-axially symmetric ones (handles and constant radius features such as decorations). The methodology applied by the authors to hundreds of real archaeological fragments (most of which were "not indicative") produced results following skilled archaeologist evaluations. The proposed results are related to analyses of high-density discretized 3D models with an average mesh size of 0.15 mm. The main limitation in the spread use of that method is the time for the acquisition and construction of a manifold model, which is, for each sherd, an average of 30 min. This time, comparable with the steps of the traditional documentation process, therefore, is incompatible with analyzing large-scale ceramic artifacts. Solutions like the "laser-aided profiler", even if they reduce documentation time drastically, still need sherds to be hand-oriented, and the drawing is based on one section of the sherd [9]. Consequently, a specific amount of variability remains, which is problematic in the statistical analysis of vessel morphometry.

Structure from Motion (SfM) 3D modeling has recently become widely used in archaeology. In [1], authors presented a new method for large-scale documentation of pottery sherds through simultaneous multiple 3D model capture using Structure from Motion. This study was based on a pilot project conducted in 2018, during which the authors recorded ceramic material from the Phoenician site of Tell el-Burak (Lebanon) using traditional methods of pottery documentation (drawing and photographing) and the new Structure from Motion (SfM). The results showed that the optimized scanning procedure allows the acquisition of each fragment in an average of 22 min. The results also showed the average time of 12 min to estimate, using commercial software, the axis of symmetry of the sherd, the representative profile, and its characteristic dimensions. The main limitation of that method is in the operator-assisted analysis of the acquired 3D models.

Despite the great utility and take up of the above-mentioned computer-based methods for documenting sites and monuments more generally, their limitations restrict their use as a standard practice for artifact documentation.

Research aims

The paper proposes a new method for a supervised automatic analysis of sherds. The proposed method represents an evolution of the corresponding acquisition and analysis methods published by the authors [1,2,7,8]. In particular, the main contributions of this paper are as follows:

- a semi-automatic acquisition method based on SfM with improvement in terms of recording quality and processing time to the published one [1];
- a computer-based method to analyze, by coding knowledge elements of archeologists, discretized models of sherds with resolutions and error levels typical of the SfM process.

The methodology’s effectiveness and applicability have been investigated by analyzing Phoenician amphora fragments from the Lebanese site of Tell el-Burak within the framework of a multidisciplinary research project based at Heidelberg University. The project, funded by the German Research Council since April 2021, aims at gaining new insights into the economy of the Phoenician homeland. One of the three main goals is the documentation and analysis of a large number of pottery sherds (c. 1800) aiming at reconstructing and understanding various aspects of the production, distribution, and consumption of Phoenician amphorae from different sites in southern Lebanon through form-typological, morphometric, and geochemical analyses. The reported results showed the potential of the proposed methodology in implementing new dimensional and morphological features, useful to introduce new hypotheses on standardization and centralization tendencies in the amphora production of the Phoenician homeland.

Materials

To test the applicability of the computed-based method on 3D models generated through SfM, a set of amphorae sherds excavated at Tell el-Burak is chosen. Phoenician amphorae have a characteristic form and can be diversified from other Iron Age amphorae produced in other parts of the Mediterranean by their elongated body with a pointed base, a pronounced shoulder carination, two handles attached to the upper part of the body, and relatively short rims (Fig. 1a). These amphorae, used to store and transport agricultural products, are directly tied to the primary production sector and can, therefore, provide important information for an investigation of ancient economies.

As Schmitt et al. 2018 [10] observed, the different morphological features of the amphorae change over time: rims are shortened, shoulder inclination declines and shoulders get thicker and shorter, and the vessels, consequently, become smaller in the later periods. For the analyses discussed in this paper, a set of 122 samples belonging to the closely related amphora subgroups A-02A, A-02B, and A-02C (Fig. 1b) have been chosen. All amphorae belonging to these subgroups have short, simple rims and, therefore, look very similar at first glance. They exhibit consistent differences, however, regarding their shoulder, which correspond to their stratigraphic origin. Amphora A-02A, the oldest type belonging to the second half of the 7th and early 6th century, has the longest and thinnest shoulders. They are replaced by A-02B, the least numerous type appearing in the 6th century, and by A-02C, the typical Persian period (6th to 4th century) amphorae [10]. Samples from all three types were included in the analysis in roughly equal amounts.

The SfM photogrammetry-based method

In order to conduct quantitative and statistical analysis, such as hypothesis testing on pottery sherds, a considerable quantity of data has to be documented due to statistical significance and relevance. This directly corresponds to longer campaigns on-site, which consequently means higher costs in the long run. Based on the previous argumentations in the introduction, such analyses are more robust, repeatable, reproducible, and extensible when applied to 3D models of the fragments.

In the last decade, photogrammetric algorithms have been developed and automated so that, combined with Structure for Motion (SfM) techniques, it has become an attractive alternative to

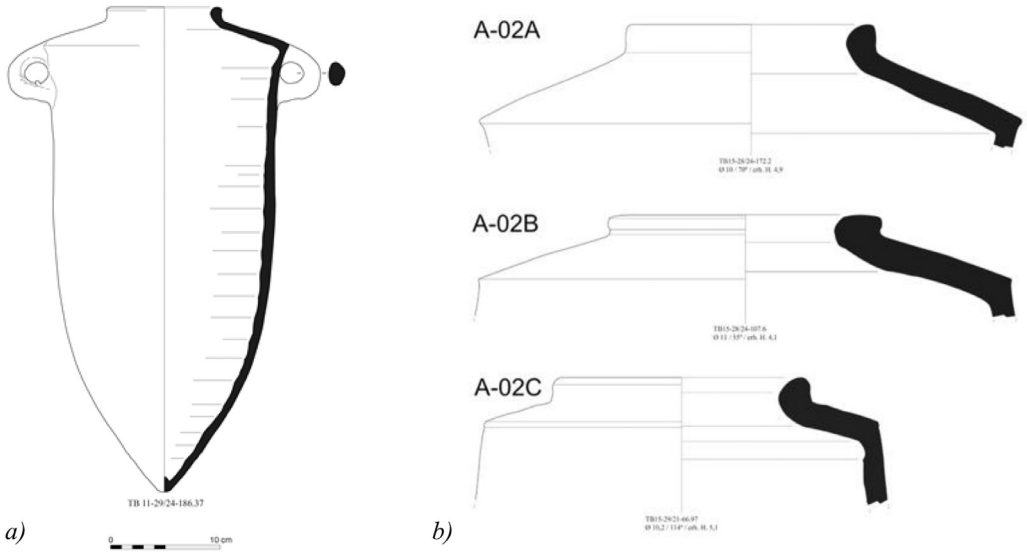

Fig. 1. a) Phoenician carinated-shoulder amphora (type A-02A) from Tell el-Burak. b) Typical examples of amphora types A-02A, A-02B and A-02C (all from Tell el-Burak).

laser scanning systems and structured light systems for large-scale complexes, statues and pottery [11–14]. SfM demonstrated robustness, reliability, accuracy, and flexibility for reconstructing small artifacts for complex morphological geometry, reflective material, or color [15]. The main weaknesses of this technique are the incomplete automation of the process and the dependence on a specialized camera operator who has to configure the camera parameters to obtain images properly focused, without blurring, and with a low noise level. If the images are not acquired adequately, the subsequent 3D reconstruction will be affected by significant noise and/or reconstruction errors, ultimately affecting object geometry.

In 2021, Göttlich et al. [1] presented a new large-scale documentation method using the 3D-capture method structure from motion to document multiple pottery sherds per shot. They argued that this documentation methodology could be significantly fast than the traditional method (based on graphical representation of sherds) while simultaneously being more affordable. Based on the criticalities mentioned above of the published method, the procedure here presented has been improved in terms of acquisition time and quality acquisition through new excavation campaigns (March 2022, November 2022, and March 2023) in Lebanon. The following briefly describes the image acquisition process and 3D reconstruction via AgiSoft Metashape, highlighting the principal introduced improvements. In a separate paper (Rummel, forthcoming), the authors will describe an in-depth analysis and discussion of the results of this campaign, a critical examination of the method, and a more extensive detailed workflow.

Generally speaking, the accuracy and reliability of the SfM final results depend on two main aspects: the acquired data quality and the experimental procedure employed for the reconstruction process. For this reason, in the proposed methodology, the "3 × 3 CPA rules" regarding geometry, camera, and procedure are employed [16,17].

Image acquisition

Fig. 2a shows the setup used. All images were acquired by a digital single-lens reflex (DSLR) camera by Nikon (D780) using a full-frame sensor with a fixed focal-length lens of 35 mm. Fig. 2b reports the technical specifications of the photogrammetric system. Fig. 2c lists the camera settings used in the performed experimentation.

The camera was mounted on a tripod. A ring light (Dörr DLR-232) was fixed to its lens. A light tent is placed on a table approximately 1 m above ground, enabling steep camera angles from below. The inner vertical sides and the bottom of the light tent are covered with a black, non-reflective cloth to provide a high-contrast background for the sherds [1]. A turntable was placed on a small box to be slightly elevated. The so-called 'pottery-tree', a stand with several clamps to hold fragments, is placed on the turntable. Seven targets were glued on the outer rim of the turntable at a distance of ca. 10–15 cm. Since these targets are essential for referencing the 3D models, their mutual distances were recorded to ensure correct referencing.

An increase in the number of clamps grows the number of documented sherds. However, too many sherds introduce unwanted overlap, reducing documented sherd surface and ultimately leading to lousy surface reconstruction. Twelve clamps are only advisable with smaller sherds. From various experiments carried out, the most efficient configuration for the sherds here analyzed has been proved as follows:

- "pottery-tree" with eight clamps;
- two above-described set-ups used simultaneously;
- two people worked on every station: one person photographed while the other prepared the next tree and repacked already documented sherds.

The photographs are taken inside a darkened room, using the ring lights mentioned above as the primary lighting source to keep similar color temperatures between photos, guaranteeing comparable lighting conditions.

After every picture was taken, the turntable was rotated by approximately 15° [1]. Consequently, every total rotation (360°) entails between 25 and 30 pictures. This guarantees an overlap of roughly 80% between adjacent images, which is the required value to reconstruct the entire surface correctly [17]. One complete revolution of the turntable required roughly between 4 and 5 min. A total of five angles or "rings", with a difference of approximately 30 cm in height, were recorded. After every repositioning or changing of elevation, the distance between the focus point and the camera was controlled again to maintain the 80 cm distance and the respective DOF of roughly 50 cm. Auto-focus is only used once to focus on the target attached to the tree (see Fig. 2c). After this, the focus is set to manual to maintain the depth of field parameters.

a)

Camera Parameters	Nikon D780
Sensor type	CMOS
Sensor size	35.9 × 23.9 mm
Pixel size [µm]	6 µm
Max Resolution	6048x4024
Effective megapixels	24.5
Focal lenght	35 cm

b)

Camera controls	Settings
Control	Manual
Auto-focus	Single focus point
ISO value	100
Aperture	f/16
Shutter speed	1/1.6 s – 1/1.4 s
Pictures format	RAW
Distance to object	80 cm[1]
DOF	ca. 50 cm

[1] Measurements were conducted between the place of focus and 35 mm in front of the cam-

c)

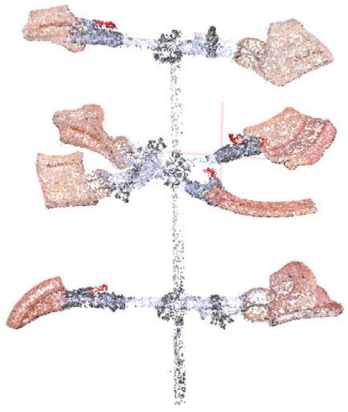

d)

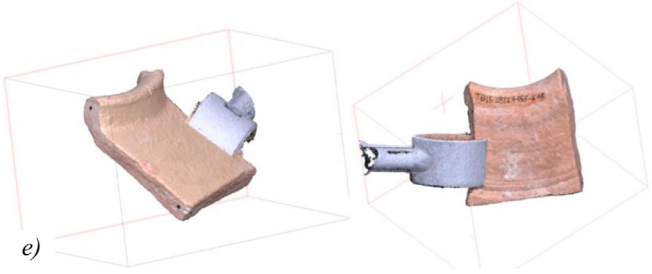

e)

f)

Fig. 2. Camera set-up and main steps of the 3D model reconstruction process. a) Set up with the camera, light tent, turntable, and pottery tree. b) Technical specifications of the photogrammetric system. c) Camera settings used in the performed experimentation. d) The sparse point cloud after aligning and cleaning unwanted noise. e) Isolated sherds and the processed dense point cloud with the clamp. f) Generated models (mesh) with a hole in correspondence of the deleted clamp.

To limit the acquisition and processing time and errors due to the registration of sherds acquired by two "pottery tree" configurations, the points covered by the clamp are neglected. When placing the fragments, the operator must position the clamp on the shoulder's fragment to avoid affecting the estimation of the dimensional features.

The last image acquisition step is capturing one picture from the middle position (ring 3 or 4) depicting an empty pottery tree in front of the black background. This picture is essential to reduce the subsequent 3D reconstruction process [1].

The presented procedure achieved optimal results with 8 to 10 trees per day, allowing each team to document 128 and 160 sherds daily. Two thousand one hundred ninety-nine pottery sherds were documented in 18 full workdays. This is significantly faster than drawing, involves fewer people, and leads to more accurate and precise documentation of the respective sherds.

3D reconstruction via AgiSoft Metashape

The following sub-chapter briefly describes the workflow for processing the data with AgiSoft Metashape, highlighting the differences with the publication [1].

Metashape is one of the most popular commercial packages for photogrammetric processing; it has a robust but straightforward workflow that can produce accurate results [18,19]. Data processing was performed as follows:

- converting pictures from RAW into TIF (16 bit) using Nikon NX Studio;
- loading the set of photos by *Add Photos* command to an empty project;
- automatically identifying the targets on the photographs by the *Detect Target's* function (tolerance: 50);

- applying image correction parameters for every ring using the *Camera Calibration* tool;
- creating a mask for the entire background by the *Import Mask* and *Create Mask from Background* tools for the entire workspace;
- aligning the pictures using the *Align photos* command (50.000 Key points – 10.000 Tie points;
- manually removing singular points and additional noise using the *Free-Form Selection* tool (Fig. 2d);
- importing reference data by creating *scale bars* with the manually documented measurements taken between the targets
- applying the *Optimized Camera (proposed parameters)* tool to recalculate the camera positions and apply the camera calibration to reference the model;
- repeat cleaning and *optimize camera* process using the *Adaptive camera model fitting* command;
- repeat cleaning and *optimize camera* process using the *Fit additional corrections* command;
- building dense point clouds by using *Build Dense Cloud* command and setting *ultra-high quality and moderate depth filtering mode*;
- removing unwanted noise by the *Editing Point Cloud* tools (Fig. 2e);
- manually removing the clamp to the model by the *Free-Form-Selection* tool;
- creating a triangular mesh by the *Build Mesh* command and setting the highest quality (Fig. 2f).

For the analysis proposed here, total reconstruction of a sherd to close the gap covered by the clamps and building texture was not carried out; this saved significant manual working time.

Compared to the workflow presented in [1], the parameters and sequence of operations were optimized to achieve the best possible quality of the final mesh. Most differences are related to technical aspects of the image acquisition and the respective functions of Agisoft, which will be discussed separately (Rummel forthcoming). From importing the pictures into AgiSoft to processing the dense clouds, the process takes roughly 45 min for one “pottery tree”. Between 10 and 15 additional minutes are needed to clean the dense clouds, choose the better pass of each sherd, cut away the clamps, and export the model. These values usually tend to reduce with the increasing experience of the processing person since this work is highly repetitive.

A Desktop-PC with an AMD Ryzen 7 (5000er series, 3.5 GHz clock rate), 64 GB RAM, and an Nvidia GeForce RTX 3060 (12 GB GDRAM) was used to generate the models and needed roughly 40 min for one dense cloud (ultra-high quality) of a model consisting of 9000–15.000 points. Larger models need, consequently, more processing time. Sixteen are rendered in roughly 10–11 h, which can be done overnight. This means that approximately two trees per day and per computer can be processed and finished.

The computer based method for automatic feature recognition

Each fragment scanned in the experimental campaign proposed in this paper has been automatically analyzed to segment and recognize the semantic and dimensional features by a computer-aided method that performs the following key steps:

- Axis identification;
- Semantic feature segmentation and recognition;
- Dimensional features evaluation.

Compared to the method published in [7], a reimplementation was necessary for analyzing meshes with a lower resolution and single-point repeatability. This method was initially developed and tested with geometric models acquired by the 3D laser scanner FARO Edge, 9 ft (2.7 m), where the single point repeatability was less than 0.064 mm, and the average point spacing of the point cloud was set to 0.15 mm. In this new version, meshes with estimated single-point repeatability of less than 0.2 mm and the average point spacing of the point cloud of approximately 0.45 mm have to be analyzed. For this purpose, some modifications are made; in the following, only substantial improvements are detailed.

Axis identification

Generally speaking, evaluating the axis of symmetry is a complex activity that affects the subsequent analysis. These difficulties arise from the availability of low-level information only from a discrete model: the points’ coordinates and the triangles’ normals. As reported in [20], this calculation is complicated in the analysis of fragments in Cultural Heritage because:

- the small fragment size limits the available information for determining the axis;
- the external surface of the fragment is only approximately axially symmetric since they are handmade objects at the wheel;
- the axially symmetric surface of an archaeological pot can be characterized by several defects due, for example, to extensive wear for weathering, encrustations, chipping, and other damage.

Added to this is, compared to the proposed experiments in [20], the sherds’ models are discretized with lower resolution and single-point repeatability. Consequently, none of the methods investigated always guarantees a reliable result.

To obtain the best axis of symmetry under the conditions considered here, this paper implemented an iterative method based on an initial solution and further refinement. The initial solution is the best one achieved by the following methods, representing state-of-the-art available to date (Fig. 3a):

- The Normal-based method [21];
- The osculating sphere-based method [22];
- The M-estimator-based method [23];
- The Circle and line fitting methods [24,25]
- The thickness versor intersection-based method [20].

The methods mentioned above use indirect properties of axisymmetric surfaces; as reported in [6], none of these methods provides accurate solutions for sherds with an incomplete circular span, especially when the density of point clouds is low and affected by micro and macro irregularities. For these reasons, the implemented procedure considers the typical manufacturing technology of ceramics, the wheel-thrown production. So, the initial solution minimizes the profile area obtained by each of these methods (highlighted in red in Fig. 3a): the profile area is calculated by the projection of the 3d coordinates of points recognized as axially symmetric in the 2D cylindrical coordinates (ρ,z), being the evaluated axis co-incident with the z-axis of the global reference system (Fig. 3b). If the surface were an exact surface of revolution and the axis was the true one, the projected profile would converge to a strict geometrical curve, and the profile area would become zero. The surface deformation (on either the macroscopic or microscopic scale) and an inaccurate axis generate a strip of projected axially symmetric points. Because of this, starting from the chosen first-attempt solution, the final one is obtained by iteratively minimizing the value of the profile area by the Levenberg-Marquardt algorithm [26].

The semantic features segmentation

Starting from a model with the axis of symmetry coincident with the z-axis of the global reference system, the semantic fea-

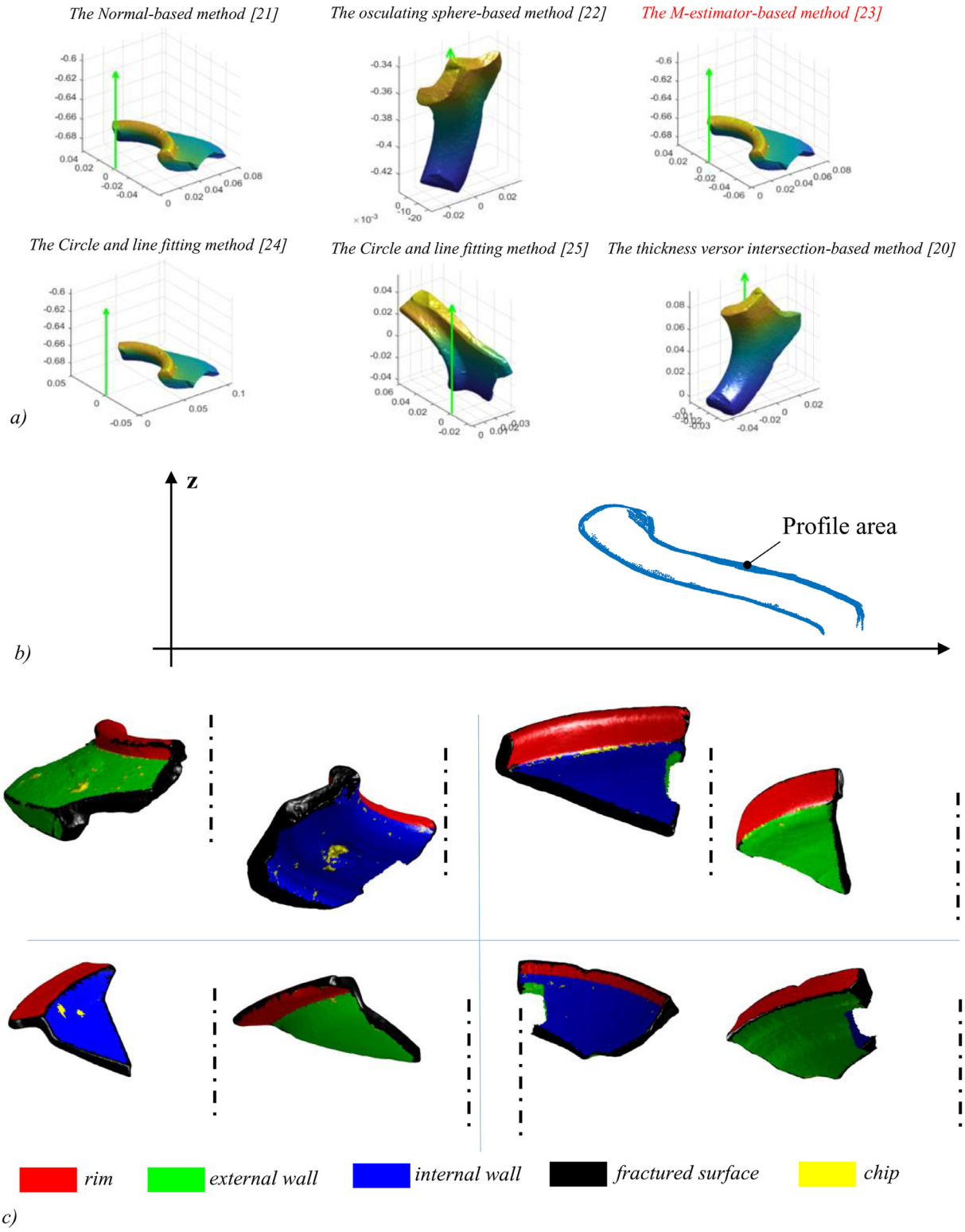

Fig. 3. Features recognition results. a) The state-of-the-art symmetry axis detection methods. b) 2D cylindrical coordinates (ρ,z) projection of the sherd model and profile area identification. c) Example of semantic feature segmentations.

tures segmentation steps are based on specifically designed rules processing geometric differential properties of discrete geometric models. According to [7], the following elements are evaluated:

- N_{ep}: number of recognized extremal parts;
- N_{fs}: number of recognized fractured surfaces;
- C_{as}: completeness of the azimuthal span;
- g: topological invariant identifying the number of holes through the object;
- g′: number of holes of the fractured surface.

Some modifications have been introduced in the implementation to consider the noisier information used in the proposed investigation.

Fig. 3c shows some examples of semantic feature segmentation of sherds acquired with the proposed scanning methodology.

The dimensional features

To characterize the amphora geometry, based on the experience of archeologists (two authors of this paper), the following dimensional features are considered in the plane z-ρ (see Fig. 3c):

- max diameter of the vessel opening (φ_O);
- the height of the rim (h_R).
- diameter of the vessel at shoulder carination (φ_S);
- the inclination of the shoulder (α_S);
- thickness of the shoulder (t_S);
- length of the shoulder (L_S).

In [2], the authors proposed a method to determine the average profile to evaluate the dimensional features, consisting of a first attempt profile identification and successful refinement. The first attempt is the profile of the radii of the circles approximating the slices perpendicular and centered on the z-axis; the refinement performs points smoothing by the parabola approximating the neighborhood of each point profile with a defined width. In preliminary experimentation, this method did not prove effective in analyzing the noisier information used in the proposed investigation. Consequently, a specifically designed procedure has been then developed to overcome these limitations and evaluate more robust dimensional features.

The proposed algorithm analyses the sections between each 3D segmented model and the sheaf of planes sharing the axis of symmetry. For each of the n_s obtained section, the above-mentioned dimensional features need the preliminary estimation of the following references:

1. The sliced points are associated with the recognized categories in the 3d (fractured surface, internal wall, external wall, rim) by the nearest point search (Fig. 4b);
2. For points associated with the external wall, normal versors are evaluated (Fig. 4c);
3. The external wall points are approximated by two straight segments (Γ_s and Γ_i); these approximations are constrained by the maximum deviation value of the normal at the points to be added (Fig. 4d);
4. The intersection point between the approximations of the external wall ($\mathbf{I}_1$) are calculated (Fig. 4e);
5. The repere points are evaluated as follows (Fig. 4f):
   - $\mathbf{P}_{MR}(\rho,z)$ is the point belonging to the slice and nearest to $\mathbf{I}_1$;
   - $\mathbf{P}_{VO}(\rho,z)$ is the point of the rim with the maximum z coordinate;
   - $\mathbf{P}_{EW}(\rho,z)$ is the point of the external wall with the maximum z coordinate.

Based on these references, the dimensional features are calculated according to the rules reported in Fig. 4g.

For each analyzed fragment and dimensional feature, by applying the rules listed in Fig. 4g, as many values as the number of sectioning planes used are obtained. Fig. 4h shows the example of the maximum vessel diameter distribution for a selected sherd; the expected and representative value is chosen as their median.

After calculating the median for each of the dimensional features, the representative profile (Fig. 4i) of the fragment is chosen as follows:

$$min\left\{\sum_{i=1}^{6} w_i \cdot \left[df_{i,j} - median\left(df_{i,j}\right)\right] \; for \; 1 \le j \le n_s\right\}$$

The hierarchical clustering of rims

Hierarchical cluster analysis refers to using some data analysis procedure to generate a hierarchical classification for an object set S [27]. For the aim of this paper, a hierarchical divisive clustering method is used: starting from a single cluster containing all observations, this is divided into more and more groups during the subsequent steps [28].

According to the results reported in literature [29,30], in this paper, the analysis is carried out by using the following five different distances between the i th (Γ_i) and j-th (Γ_j) profiles:

- Euclidean distance: $d_E(\Gamma_i,\Gamma_j) = \frac{1}{|\Gamma_i|}\sum_{\boldsymbol{p}_h\in\Gamma_i}\|\boldsymbol{p}_h - \boldsymbol{q}_h\|_2$ with $\boldsymbol{q}_h \in \Gamma_j$;
- Haussdorff distance: $d_H(\Gamma_i,\Gamma_j) = \max_{\boldsymbol{p}_h\in\Gamma_i}\{\min_{\boldsymbol{q}_k\in\Gamma_j}\|\boldsymbol{p}_h - \boldsymbol{q}_k\|_2\}$;
- Chamfer distance: $d_{CD}(\Gamma_i,\Gamma_j) = \frac{1}{|\Gamma_i|}\sum_{\boldsymbol{p}_h\in\Gamma_i}\min_{\boldsymbol{q}_k\in\Gamma_j}\|\boldsymbol{p}_h - \boldsymbol{q}_k\|_2 + \frac{1}{|\Gamma_j|}\sum_{\boldsymbol{q}_k\in\Gamma_j}\min_{\boldsymbol{p}_h\in\Gamma_i}\|\boldsymbol{q}_k - \boldsymbol{p}_h\|_2$;
- Earth Mover's distance: $d_{EMD}(\Gamma_i,\Gamma_j) = \min_{\varphi:\Gamma_i\to\Gamma_j}\sum_{\boldsymbol{p}_h\in\Gamma_i}\|\boldsymbol{p}_h - \varphi(\boldsymbol{p}_h)\|_2$ where the bijection mapping φ is found by solving an optimization problem;
- Profiles distance: $d_p(\Gamma_i,\Gamma_j) = \frac{\omega_R}{\langle R\rangle}d_R(\Gamma_i,\Gamma_j) + \frac{\omega_\vartheta}{\langle\vartheta\rangle}d_\vartheta(\Gamma_i,\Gamma_j) + \frac{\omega_k}{\langle k\rangle}d_k(\Gamma_i,\Gamma_j)$.

The profile distance evaluation is carried out according to [30]. To cluster the rims based on the shape and to reduce the effect of different rim dimensions and discretization, each representative profile is scaled to the rim height and is discretized uniformly using a spline approximation.

For each proximity index, the number of components of observations is obtained by manipulating the distance matrix using the PCA analysis; this makes it possible to order the columns in terms of total variability within the assemblage. In this paper, according to the results reported in [30], the number of components is obtained by the following constraints:

1. The included components have to represent more than 90% of variability;
2. Each selected component corresponds to at least 2% of the total variability;
3. All components contributing more than 5% are included, even if the cumulative variability exceeds 90%.

The results of the hierarchical cluster analysis are graphically represented by a dendrogram that shows at which distance observations are divided.

Results

The proposed computer-based method (in the following *Keramodeo V1.1*) was implemented in the original software coded in MATLAB. Particular efforts in the implementation have been addressed to limit user interaction.

The automatic analysis method requires the input of the parameters listed in Fig. 5a; these values were set through a preliminary experiment on five amphora fragments acquired with the proposed SfM-based method and chosen randomly. All other required parameters are set up based on the results obtained from publications in the literature [7,20].

The first elaboration is carried out to evaluate the discrete differential properties at each vertex and the symmetry axis for each sherd recorded in the analyzed directory (Fig. 5b). For every fragment (*Sherdname(i).stl*), the following files are saved:

- *sherdname(i).ddf*: an ASCII file containing the coordinate and the discrete differential properties of each vertex and pointer to vertices of the triangular tessellation;

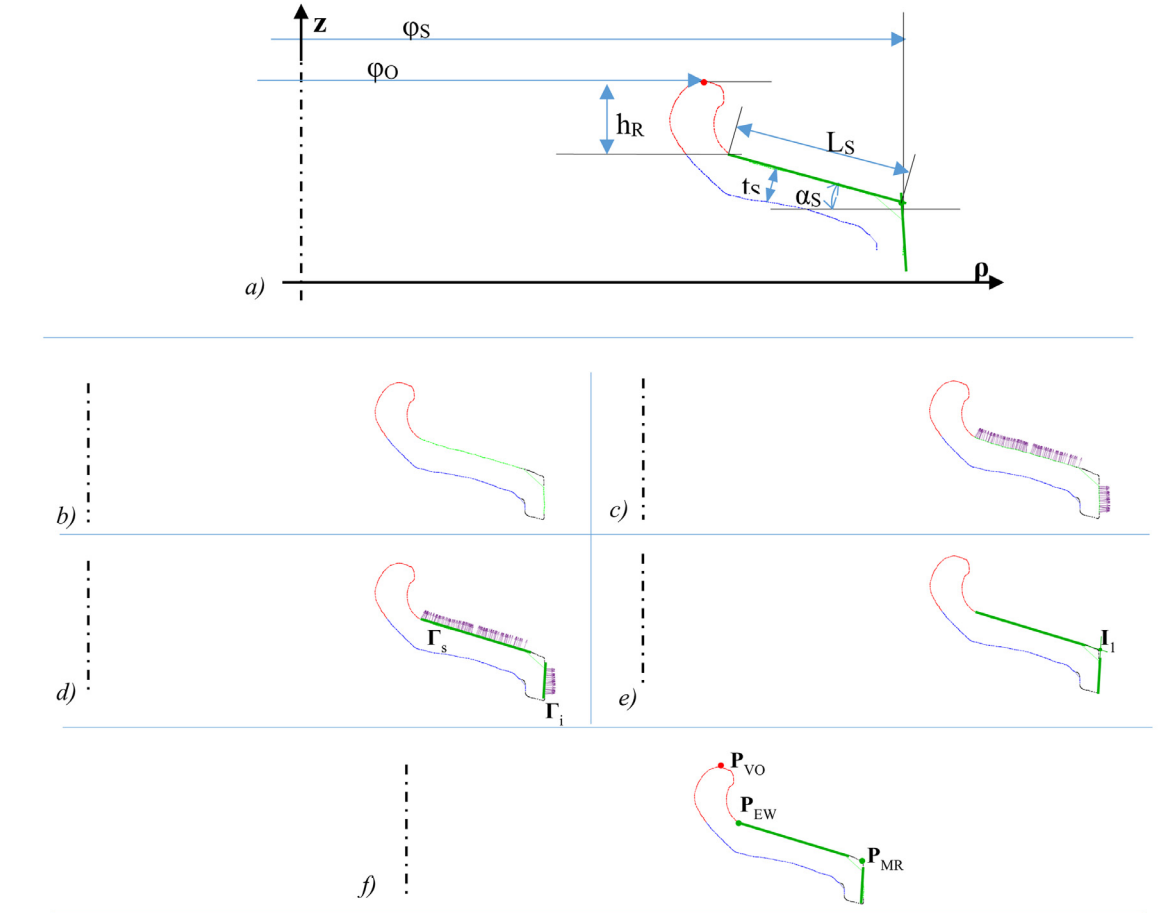

Dimensional feature	rule
max opening of vessel	$2 * \rho_{P_{VO}}$
height of the rim	$z_{P_{VO}} - z_{P_{EW}}$
max diameter of vessel at shoulder carination	$2 * \rho_{P_{MR}}$
inclination of vessel shoulder	$acos(\Gamma_s \cdot \rho)$; *angle respect to the horizontal of* Γ_S
thickness of vessel shoulder	*median value of the minimum distance between the internal and external wall approximated by* Γ_S
lenght of vessel shoulder	$\overline{P_{EW}P_{MR}} \cdot \Gamma_s$; *distance between* P_{EW} *and* P_{MR} *along* Γ_S

g)

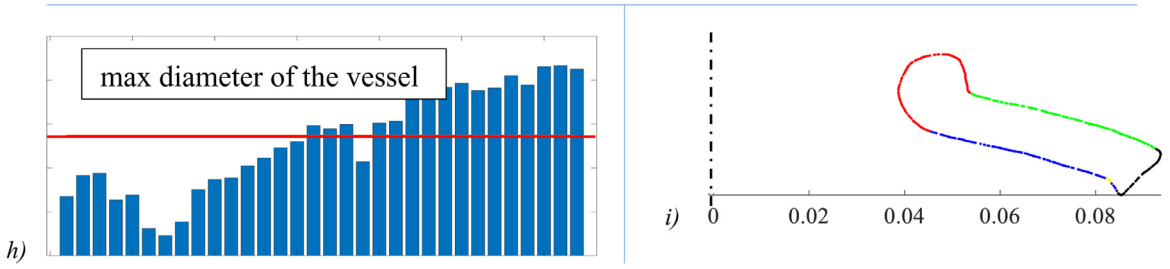

Fig. 4. Main steps of dimensional features estimation process. a) Parameters here analyzed to characterize the amphora geometry. b) Sliced points associated with the recognized categories in the 3d. c) Normal versors at points associated with the external wall. d) External wall points approximation by two straight segments (Γ_s and Γ_i). e) Intersections I_1 between Γ_s and Γ_i. f) Repere points. g) The implemented rules to evaluate the dimensional features of amphora h) Example results of the analysis for each section of the segmented sherd and the corresponding representative value for the dimensional feature (red line). i) Example of representative fragment profile.

- *sherdname(i)_axis.dat*: an ASCII file with the anchorage point coordinates and the versor of the symmetry axis;
- *sherd-name(i)_axis.fig*: a MATLAB figure depicting the axis detection results for each analyzed method.

Once the processing is finished, the operator can view all the images related to the analyzed fragments (Fig. 5c), modify the parameters, and re-launch the calculation for those fragments for which the estimation axis failed.

a)

Automatic method steps	*parameters*	*description*	*value*
Discrete differential properties evaluation	n_h	*Neighbourhood order*	*3*
Axis estimation	τ_{SHI}	*Smoothness indicator threshold value*	*0.02*
	mn_p	*Minimum region points*	*100*
The semantic features segmentation	τ_{SHI}	*Smoothness indicator threshold value*	*0.02*
	$\tau_{distance}$	*Point axis threshold value*	*10*
	mn_p	*Minimum size patch*	*500*
	mn_{uep}	*Minimum size upper extremes*	100
	mn_{lep}	*Minimum size lower extremes*	100
	τ_{rim}	*Fragment height range for rim detection*	$(\zeta_{max} - \zeta_{min})/5$

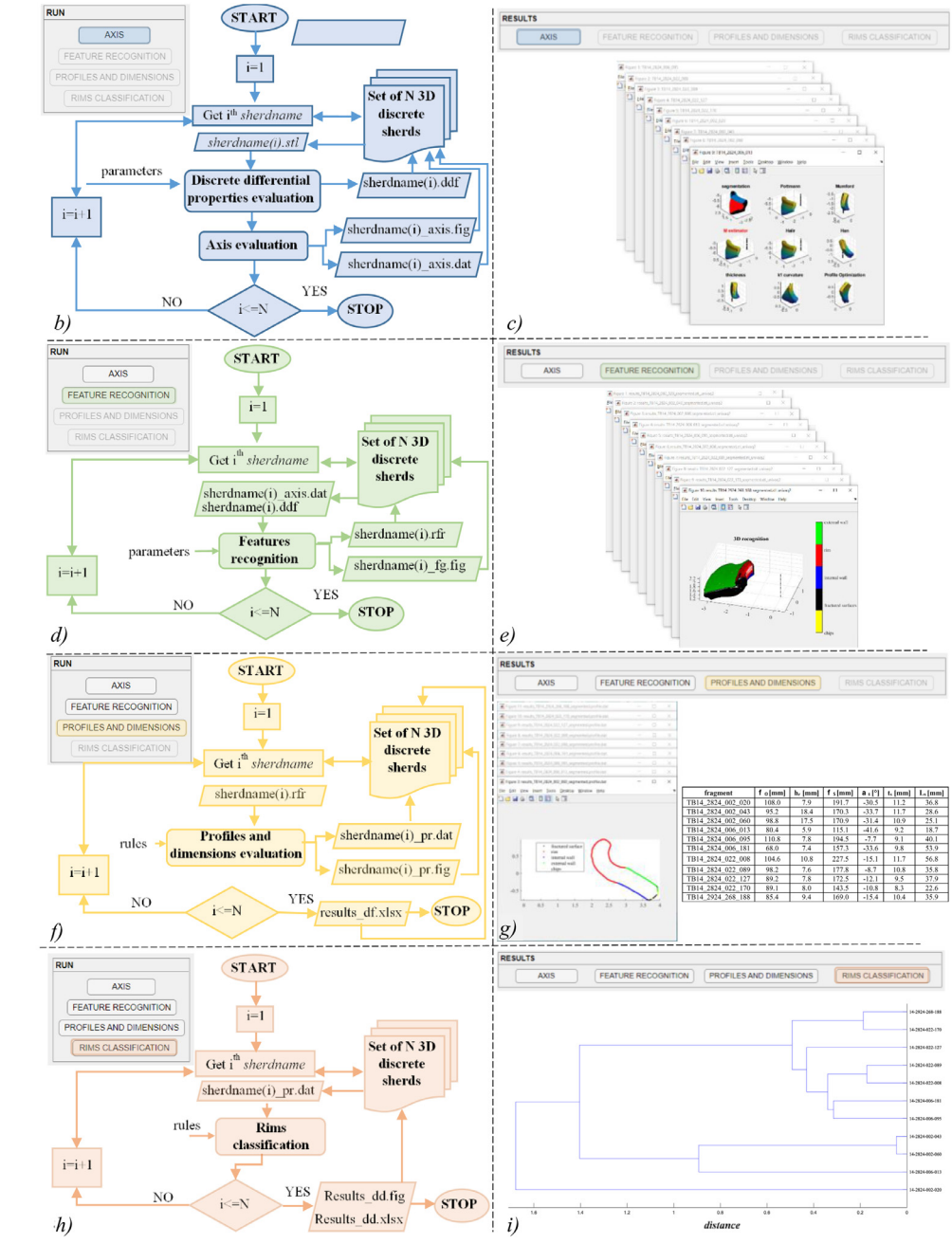

Fig. 5. Keramodeo V1.1 input parameters and working principle flow-chart.

The second step of the proposed method concerns the segmentation and recognition of the morphological and geometrical features for each sherd recorded in the analyzed directory (Fig. 5d). For every fragment (*sherdname(i).stl*), the following files are saved:

- *sherdname(i).rfr*: an ASCII file containing the feature recognition and segmentation results according to the file format reported in [7];
- *sherd-name(i)_fg.fig*: a MATLAB figure depicting the feature recognition and segmentation results.

a)

	A-02	Mean	Median	Min	Max	Std Dev	CV	N
φ_O [mm]	A	92.4	91.4	69.7	148.3	13.3	14.4%	41
	B	107.3	104.8	77.0	144.0	13.8	12.8%	42
	C	101.3	98.5	76.5	144.7	13.1	12.9%	39
h_R [mm]	A	12.6	12.3	8.6	22.6	2.4	19.1%	41
	B	8.2	7.9	5.1	14.2	1.6	19.7%	42
	C	9.4	9.5	3.9	13.9	2.3	24.5%	39
α_S [°]	A	-20.8	-21.2	-27.5	-13.7	3.6	-17.5%	41
	B	-20.1	-20.1	-37.8	-1.7	5.4	-26.9%	42
	C	-12.2	-11.8	-25.9	0.2	6.0	49.2%	39
t_S [mm]	A	8.9	8.7	5.6	13.5	1.4	15.9%	41
	B	11.8	11.8	9.2	18.1	1.8	14.9%	42
	C	11.2	10.7	8.6	19.0	2.0	17.7%	39
φ_S [mm]	A	220.0	211.1	179.5	264.6	27.2	12.4%	7
	B	225.6	223.2	192.2	292.3	26.1	11.6%	20
	C	181.8	176.4	155.1	251.7	20.8	11.4%	29
L_S [mm]	A	62.9	61.0	51.0	84.8	10.6	16.9%	7
	B	63.0	61.4	44.9	92.2	12.5	19.9%	20
	C	38.5	36.2	20.7	64.8	10.5	27.2%	29

b)

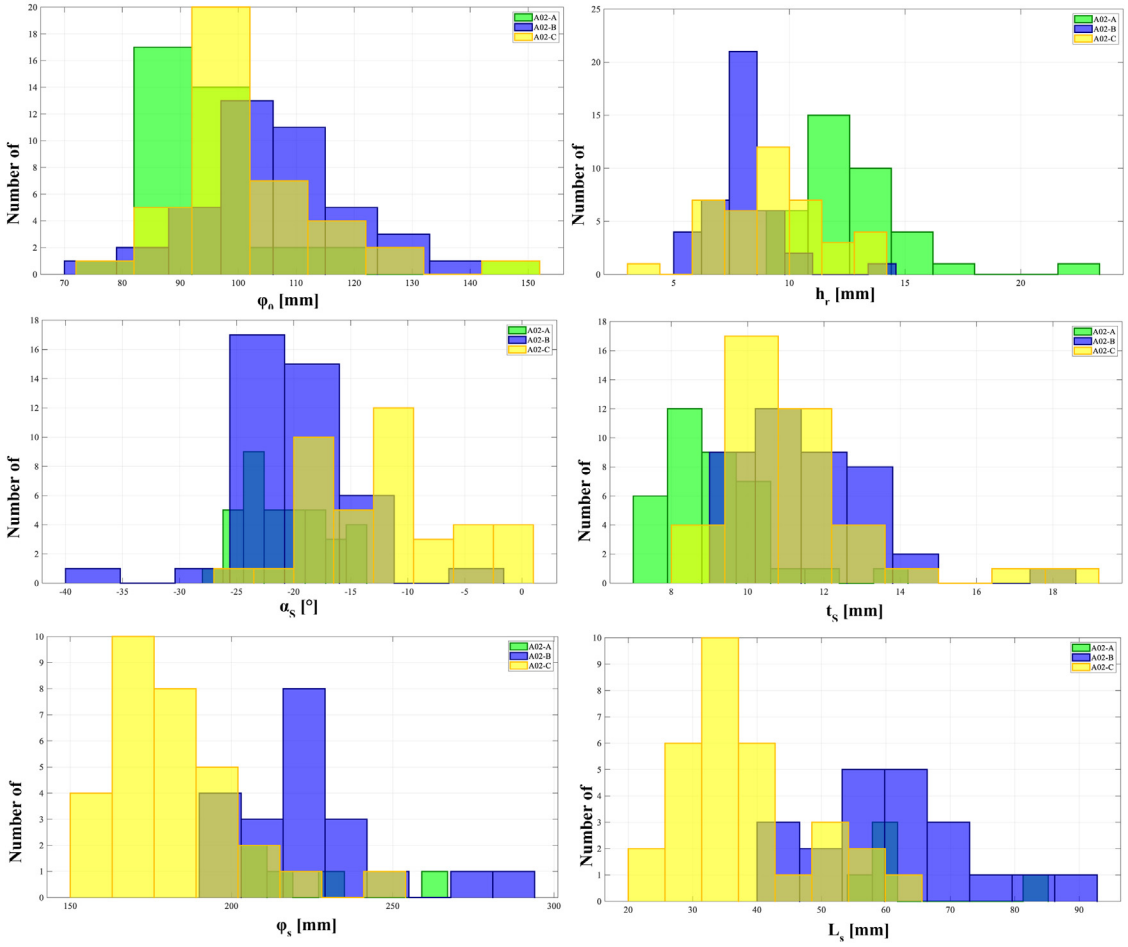

Fig. 6. Results of the dimensional features here considered for the 122 analyzed sherds. a) Statistical analysis. b) Distributions (b).

The archaeologist can check the images of the segmentation results for all analyzed fragments (Fig. 5e) and identify unsatisfactory analyses; for them, the input parameters must be modified and the simulation re-launched.

The last two phases concern the dimensional features, representative profile evaluations (Fig. 5f), and the rims clusterization (Fig. 5h). The proposed implementation allows for the visualization of the results for the last two phases (Fig. 5g and i).

Statistical analysis of measured vessel features and interpretation of results

The first experiment concerned the statistical analysis of the dimensional features reported in section 4.3 for 122 sherds presented in section 2. The values obtained for the average mesh size (in almost all cases less than 0.75 mm) allow analyzing the dimensional features, here considered, having characteristic dimensions

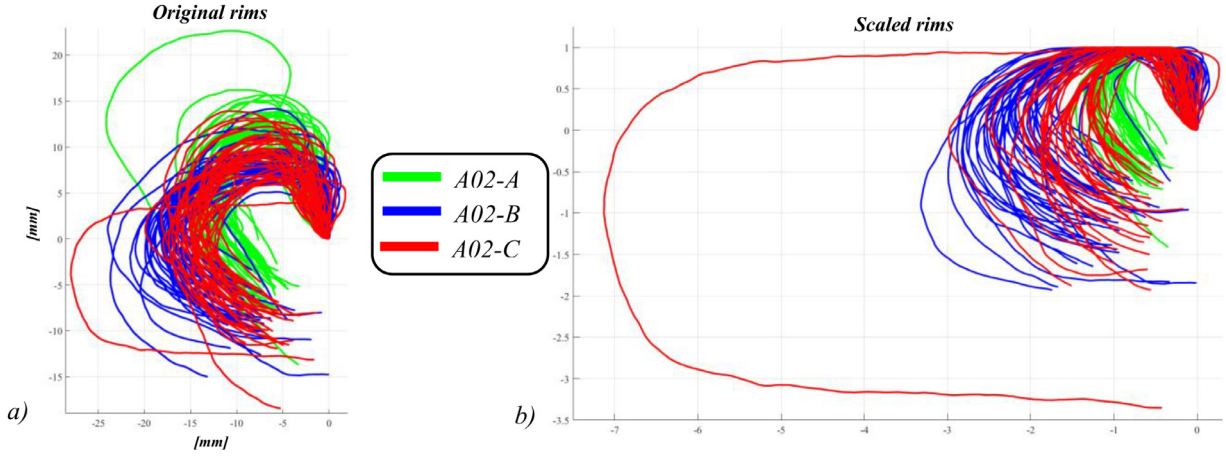

Fig. 7. Representation of the recognized rims.

of the order of magnitude of 10 mm. The operator and archaeologist's direct interaction in the sherds' analysis was timed: the average value obtained was about six minutes per sherd. The calculation times for obtaining the results of the different steps were not monitored: they were not considered significant since the used implementation was in the prototype stage.

The automatically generated values (see Tables in supplementary materials) were submitted to statistical analysis using the JMP software (Fig. 6a). The values of φ_S and L_S are evaluated only for fragments with completely preserved shoulder (i. e. until shoulder carination). As the sample set is small (37 samples for A-02A, 41 for A-02B, and 39 for A-02C), the results and the following interpretation should be considered preliminary.

The orifice diameter values (φ_O) are very similar. Pragmatic reasons most convincingly explain this. The vessel opening was wide enough to allow an adult male hand to enter the vessel during manufacture and use (e. g. coating with resin, retrieval of content, and cleaning).

The height of rims (h_R) is reduced from 12.6 mm in A-02A to 8.2 mm in A-02B and 9.4 mm in A-02C. Rim height is highly standardized, indicated by low values for standard deviation. So far, there is no convincing hypothesis to explain the reduction in rim height.

A-02A and A-02B amphorae shoulders do not differ much in length (L_S), while is sharply reduced by almost half in A-02C amphorae. The standard deviation is low and nearly identical for each type indicating a high degree of standardization. Interestingly, shoulder thickness (t_S) is increased with the reduction of shoulder length. A-02B shoulders are slightly shorter and, on average, 3 mm thicker than A-02A shoulders. The thicker shoulders are retained in A-02C even though shoulder length is reduced. The changes in these two factors (L_S and t_S) indicate an intention to produce sturdier vessels less prone to breakage during handling and probably especially transport on ships. The decline in shoulder inclination (α_S) might also have resulted from these changes in amphora production. The reduction of shoulder length causes a decrease in the maximum shoulder width (φ_S) and, most likely, a reduction in overall vessel size. Standard deviation and coefficient of variation are relatively high for φ_S in all three amphorae types. This might be taken as an indication of several standardized capacities if maximal shoulder diameter indicates overall vessel size. However, this hypothesis needs to be checked on a more extensive sample set. The decrease in vessel size correlates with introducing of a new type of handle. Both changes, smaller amphorae and new handle forms, were probably introduced to facilitate amphora transport by human carriers (cf. Rönnberg and Schmitt, forthcoming).

The qualitative analysis of Fig. 6a resulted in similar conclusions to those obtained in [10], although different fragments belonging to categories A02-A and A02-B were analyzed. The proposed methodology results allow replicating archaeologists' general considerations, based on the traditional method, for Phoenician carinated-shoulder amphorae. This, however, is achieved more quickly, economically, repeatably, reproducibly, and easily expandable to new types of recognized feature analysis. Fig. 6b shows the distribution of the dimensional feature considered for the three typologies of analyzed amphorae. Although the above considerations on values can be drawn on, none of the six parameters can be used to cluster unambiguously fragments in one of three specific groups.

Automated hierarchical rims classification

The second experiment concerns applying the hierarchical clustering method of rims presented in section 4.4. The aim was to obtain computer-based clustering of the analyzed amphora sherds independent of the conventional vessel grouping (A-02A, A-02B, A-02C) as suggested by the involved archaeologists.

Fig. 7 shows the representation of the original recognized rims (Fig. 7a) and those scaled on the rim height (Fig. 7b) for the three categories considered here. The origin of each rim is positioned at the point closest to the external wall.

The first cluster analysis was carried out for each sherd category to investigate the presence of sherds belonging to the same vessel or traceable to a similar form of the rim. For this reason, the Euclidean,

Haussdorff, Chamfer and the Earth Mover's distances were used as the proximity index (Fig. 8). For each of the three categories, the figure also shows the pairs of profiles recognized as most similar for the four metrics used and their respective values of dimensional features considered here. Fig. 8 shows differences in the similarity detection for the categories A2B and A2C obtained using diverse metrics; furthermore, none of the fragment pairs recognized as most similar belong to the same shard.

Fig. 9 compares cluster dendrogram results using all the five distance metrics here considered (Fig. 9a: Euclidean distance, Fig. 9b: Haussdorff distance, Fig. 9c: Chamfer distance, Fig. 9d: The Earth Mover's distance and Fig. 9e: profile distance). The identifiers of the respective fragments are coloured according to the three categories considered (A02-A: green; A02-B: blue; A02-C: red).

Using the distance profile as a proximity index and the presented procedure to determine the number of groups, the process clusters the 122 fragments into three groups: one for A02-A, one for A02-B, and one for A02-C. Calculating the profile dis-

A02-A

Distance metric	Frammento ID	φ_O [mm]	h_R [mm]	α_S [°]	t_S [mm]	L_S [mm]	φ_S [mm]
Euclidean Hausdorff Chamfer The Earth Mover's	2922-013-0008	85.9	13.8	-24.8	8.5	60.9	209.5
	2922-013-0061	115.6	15.0	-20.8	9.2		

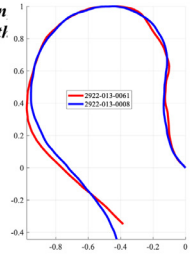

A02-B

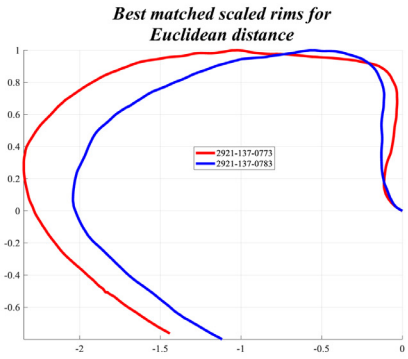

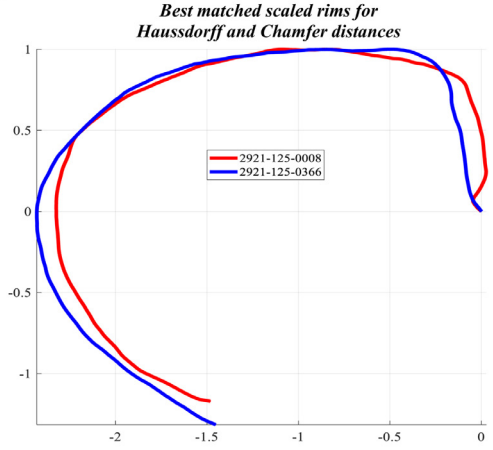

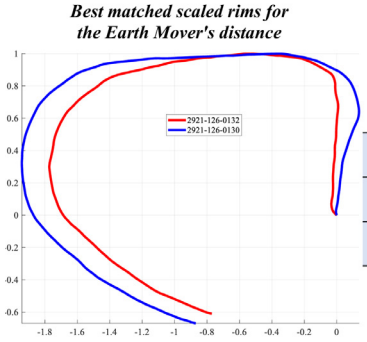

Distance metric	Frammento ID	φ_O [mm]	h_R [mm]	α_S [°]	t_S [mm]	L_S [mm]	φ_S [mm]
Euclidean	2921-137-0773	107.1	7.9	237.1	-15.5	12.4	63.7
	2921-137-0783	103.6	8.3	195.3	-18.6	12.2	44.9
Haussdorff Chamfer	2921-125-0008	104.8	7.7	219.6	-20.6	12.2	58.0
	2921-125-0366	108.7	6.5		-25.3	12.6	
The Earth Mover's	2921-126-0130	118.0	9.3		-20.8	10.5	
	2921-126-0132	103.6	9.5	228.8	-21.8	11.1	61.9

A02-C

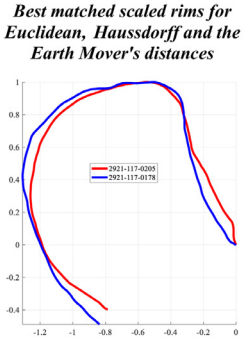

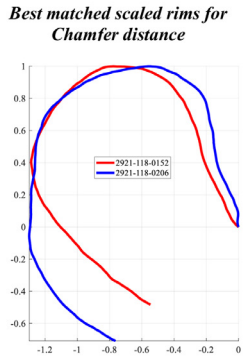

Distance metric	Frammento ID	φ_O [mm]	h_R [mm]	α_S [°]	t_S [mm]	L_S [mm]	φ_S [mm]
Euclidean, Haussdorff The Earth Mover's	2921-117-0178	88.4	10.8	155.7	-2.1	10.3	27.3
	2921-117-0205	117.0	12.2	186.6	-5.3	11.2	26.8
Chamfer	2921-117-0152	96.3	13.9	176.8	-16.0	10.5	34.2
	2921-117-0206	100.2	12.2	191.7	-11.8	12.8	42.1

Fig. 8. Results of the hierarchical cluster analysis by using the Euclidean distance and analyzing the categories fragments separately.

tance proved to be the best approach as it delivered results consistent with the grouping done by the archaeologists. This outcome demonstrates the potentialities of a new reliable method to group pottery vessels corresponding with human perception that can be used as an independent tool to cluster significant form typologies.

Comparison of amphora profiles: conventional drawings vs. automated method

A third experiment concerned the comparison in the analysis of Phoenician amphora fragments between the application of the traditional method [10] and the proposed one. In particular,

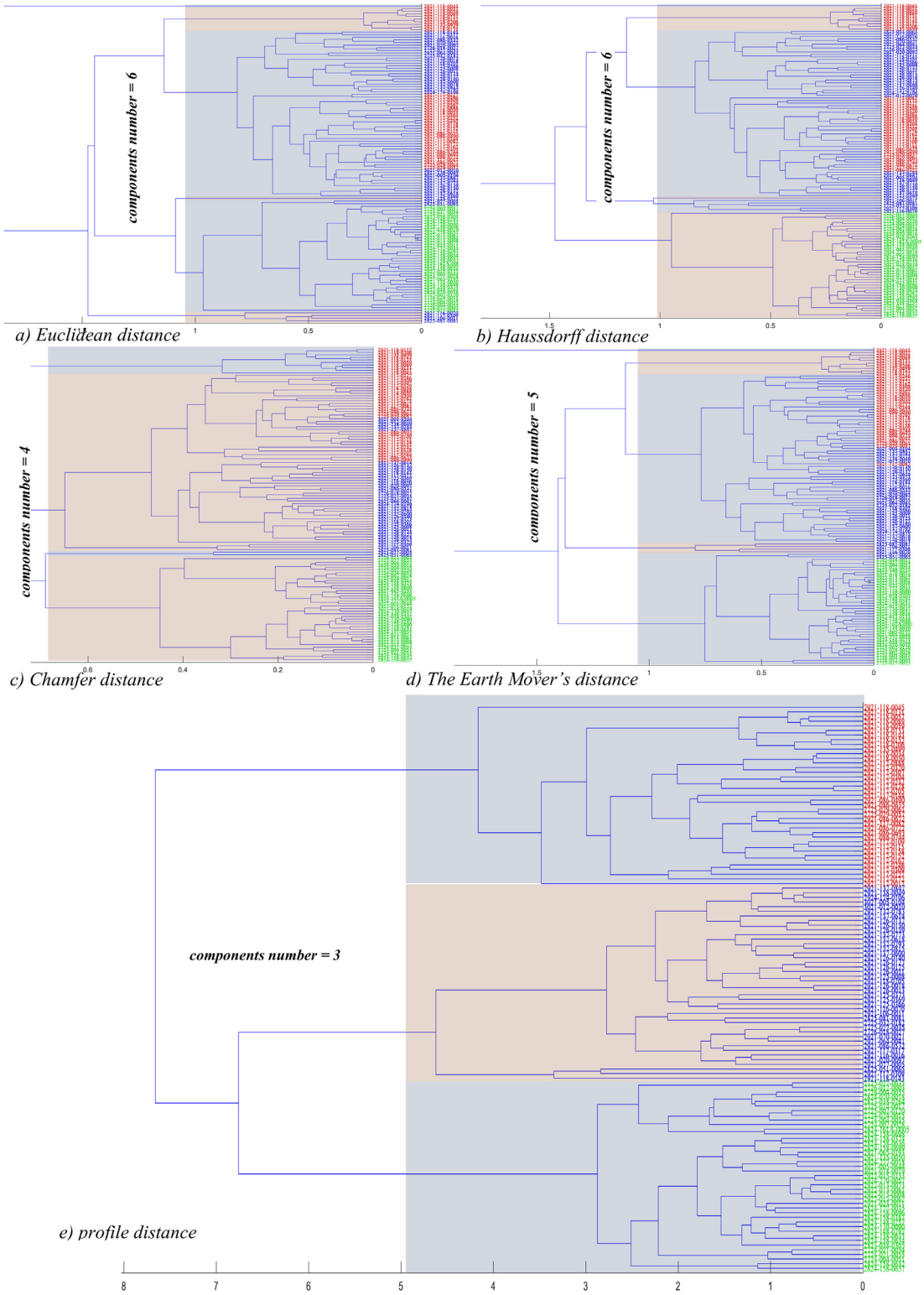

Fig. 9. Results of the hierarchical cluster analysis by using the Euclidean (a) and profile distance (b), analyzing all the 122 fragments.

11 fragments belonging to the three categories considered here (A02-A, A02-B, and A02-C) were analyzed from all the 3D models available at the following link (https://www.tandfonline.com/doi/suppl/10.1080/00758914.2018.1547004?scroll=top&role=tab). For each downloaded fragment, the following materials were provided:

- The values of the dimensional features considered here, obtained by the manual method;
- The drawings of the calibrated profiles;
- The 3D models.

Fig. 10a compares the profiles obtained from the archaeologists' drawings and those of the proposed automatic system. The difficulties of the even experienced archaeologist in aligning the fragment in the 3d space are evident. This causes different values of the considered dimensional features. Fig. 10b shows the percent-

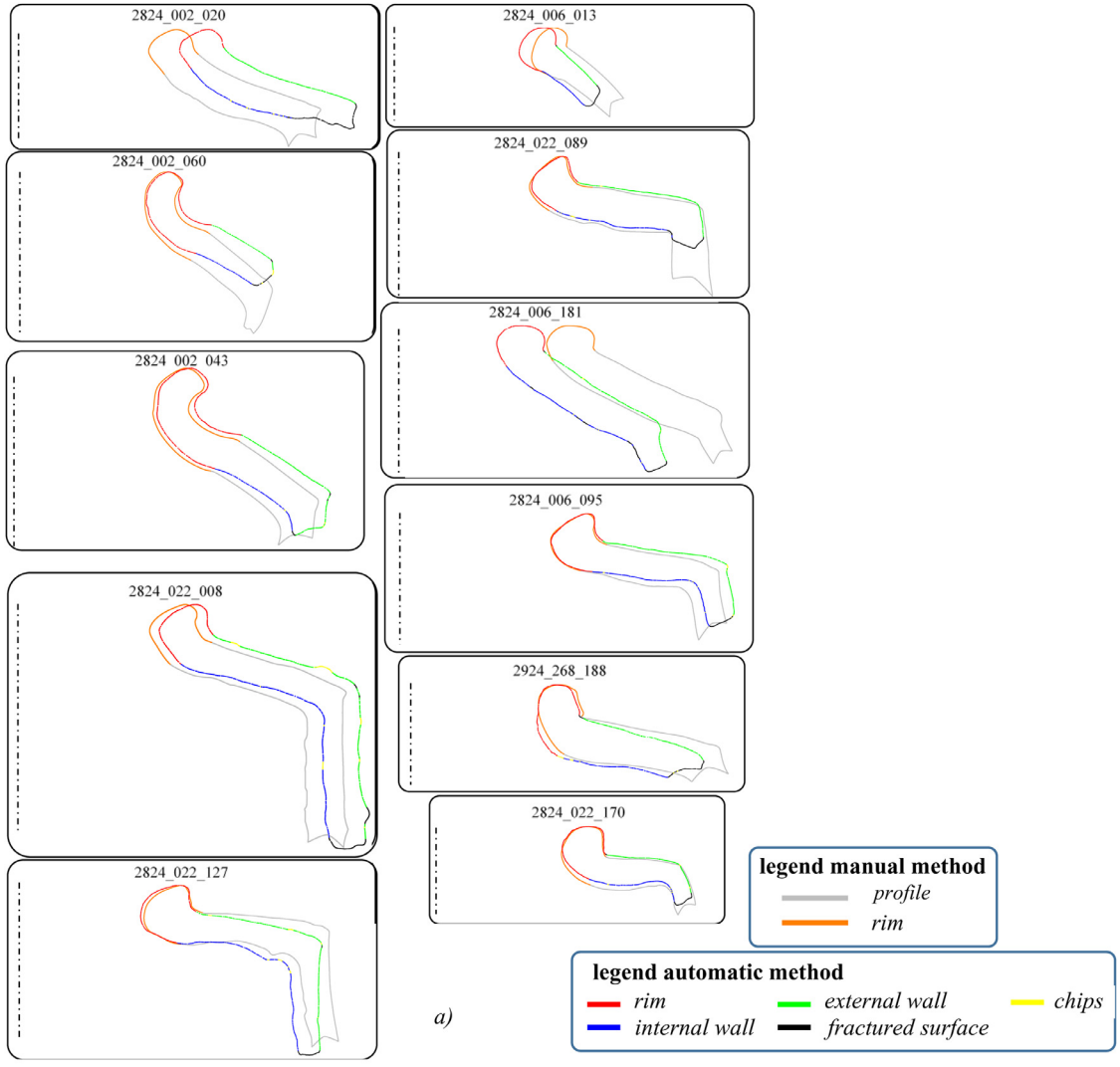

b)

fragment name	φ_o	h_r	α_s	t_s	φ_s	l_s
2824_002_020	19.96%	12.29%	17.27%	2.03%		
2824_002_043	3.46%	8.09%	4.48%	6.34%	17.19%	2.30%
2824_002_060	2.92%	12.51%	21.60%	8.63%	3.60%	0.26%
2824_006_013	6.53%	1.67%	0.99%	2.55%		
2824_006_095	0.75%	13.48%	48.34%	9.41%	3.47%	8.46%
2824_006_181	27.62%	5.56%	15.45%	24.49%	11.03%	25.35%
2824_022_008	6.71%	1.94%	28.19%	6.64%	17.88%	23.48%
2824_022_089	2.28%	15.60%	21.19%	9.88%	2.83%	5.71%
2824_022_127	0.85%	2.34%	3.65%	21.03%	13.21%	5.18%
2824_022_170	1.31%	11.60%	54.46%	17.24%	2.39%	1.54%
2924_268_188	1.88%	4.67%	18.66%	4.13%		

Fig. 10. Comparison between the manually drafted and automatic derived profiles for eleven profiles available from https://www.tandfonline.com/doi/suppl/10.1080/00758914.2018.1547004?scroll=top&role=tab.

age differences for each dimensional feature to investigate this aspect. The most significant average differences are obtained, as was to be expected, for α_s and t_s: for α_s, this stems from the previously exposed difficulty of positioning the profile in 3D space, for t_s, from the intrinsic difficulty of assessing with a gauge the thickness, which is generally variable along the profile.

Conclusions and discussion

Traditionally, archeological research, archive management, conservation, exhibition, and utilization techniques are based on manual activities and analyses performed by skilled operators. Due to limitations of the traditional method, the recommendations of

"UNESCO, ICCROM, ICOMOS (1994)" on preserving the authenticity and integrity of archaeological excavations and finds have not yet been satisfactorily achieved.

For this purpose, the development of digital methods for documenting archaeological artifacts has been given much attention over the last three decades. Despite the scientific community's efforts, no computer-based method proved effective in analyzing large quantities of fragments for the following reasons:

- 3D model acquisition times are not compatible with the analysis of large quantities of material,
- features recognized cannot be associated with those considered by archaeologists.

Several specific skills must be harnessed to contribute effectively to this area and overcome state-of-the-art limitations. For this purpose, a new international research group was formed, consisting of archaeologists with specific skills and experience in fast 3D geometry acquisition methods and researchers who developed and published the only available computer-based process of recognizing the more significant geometric and morphological sherds features analyzed by archaeologists. This collaboration resulted in the fully digital methodology proposed in the paper that proved to have the potential to analyze large amounts of ceramic material and to produce meaningful results through the automated analysis of various parameters.

The proposed methodology consists of two main parts:

1. 3D acquisition of sherds with the construction of the discrete 3D manifold model;
2. recognition, segmentation, and dimensional characterization of morphological and geometrical features of a specific typology of ceramic finds.

The 3D model acquisition is based on the Structure from Motion technology, allowing simultaneous capture of information of multiple sherds, saving time and resources, and being not dependent on a constant supply of electricity. The 3D models are then generated using AgiSoft Metashape, one of the most popular commercial packages for photogrammetric processing.

The automatic method is based on a specifically designed analysis of the discrete geometric differential properties and geometric and topological invariants of the 3-D model.

Compared to the methods presented by the authors in previous papers [1,2,7,8], several improvements are proposed; the most important ones are:

- optimization and speeding up of the acquisition process;
- hardening algorithms to analyze discrete models with a poorer resolution and higher noise level;
- codifying piece of the archaeologists' knowledge in the recognition and dimensional characterization of semantic features used to characterize a specific family of ceramic fragments.

The method was applied to analyze a set of 122 Phoenician amphorae sherds excavated at Tell el-Burak (Lebanon). Only fragments that underwent recognizable and quantifiable changes within the late Iron Age and Persian Period were chosen for this pilot study. Compared to the sherds analyzed in [10], the ones presented here consider A-02B samples for the first time, whereas the earlier A-01 amphorae were excluded.

The method demonstrated the potential to analyze large quantities of sherds, generating the same knowledge elements used by archaeologists to characterize the sherds considered here in a more robust, repeatable, and reproducible way. It also showed the potential to implement new knowledge elements to analyze ceramic finds by generating high-level information from those acquired from 3D models. The improvements introduced with the proposed automatic methodology was confirmed by comparing the statistical analysis results with those of a previous study [10].

Future efforts will be focused on further improvement and development of the presented method, on using this methodology to analyze large quantities of fragments, and on the complete sharing of the gained knowledge and generated data. For this purpose, more configurations of the experimental setup will be tested to reduce the time, equipment cost, and human labor hours, enhancing the acquisition quality. The computer-based analysis method will be improved by implementing original strategies to determine automatically, for each fragment, the corresponding parameters τ_{SHI} and τ_{rim}. This will reduce the operator supervision in evaluating the results in symmetry axis and segmentation estimations.

Finally, having verified the method's potential in this paper, several hundred samples of A-01 and A-02 amphorae excavated at different Phoenician sites will be investigated to obtain a statistically significant analysis to derive new hypotheses on the differentiation among various production sites.

Supplementary materials

Supplementary material associated with this article can be found, in the online version, at doi:10.1016/j.culher.2024.03.012.

References

[1] F. Göttlich, A. Schmitt, A. Kilian, H. Gries, K. Badreshany, A new method for the large-scale documentation of pottery sherds through simultaneous multiple 3D model capture using structure from motion: Phoenician carinated-shoulder amphorae from Tell el-Burak (Lebanon) as a case study, Open Archaeol. 7 (1) (2021) 256–272.
[2] L. Di Angelo, P. Di Stefano, C. Pane, An automatic method for pottery fragments analysis, Measurement 128 (2018) 138–148.
[3] A. Gilboa, A. Tal, I. Shimshoni, M. Kolomenkin, Computer-based, automatic recording and illustration of complex archaeological artifacts, J. Archaeol. Sci. 40 (2) (2013) 1329–1339.
[4] D. Tanasi, The digital (within) archaeology. Analysis of a phenomenon, Historian 82 (1) (2020) 22–36.
[5] C. Morgan, Current digital archaeology, Annu. Rev. Anthropol. 51 (2022) 213–231.
[6] L. Di Angelo, P. Di Stefano, E. Guardiani, A review of computer-based methods for classification and reconstruction of 3D high-density scanned archaeological pottery, J. Cult. Herit. 56 (2022) 10–24.
[7] L. Di Angelo, P. Di Stefano, E. Guardiani, C. Pane, Automatic shape feature recognition for ceramic finds, J. Comput. Cult. Herit. (JOCCH) 13 (3) (2020) 1–21.
[8] L. Di Angelo, P. Di Stefano, A.E. Morabito, C. Pane, Measurement of constant radius geometric features in archaeological pottery, Measurement: J. Int. Meas. Confederat. 124 (2018) 138–146.
[9] P. Demján, P. Pavúk, C.H. Roosevelt, Laser-aided profile measurement and cluster analysis of ceramic shapes, J. Field. Archaeol. (2022) 1–18.
[10] A. Schmitt, K. Badreshany, E. Tachatou, H. Sader, Insights into the economic organization of the Phoenician homeland: a multi-disciplinary investigation of the later Iron Age II and Persian period Phoenician amphorae from Tell el-Burak, Levant 50 (1) (2018) 52–90.
[11] M. Rodríguez-Martín, P. Rodríguez-Gonzálvez, Suitability of automatic photogrammetric reconstruction configurations for small archaeological remains, Sensors 20 (10) (2020) 2936.
[12] F. Avella, V. Sacco, F. Spatafora, E. Pezzini, D. Siragusa, Low cost system for visualization and exhibition of pottery finds in archeological museums, SCIRES-IT - SCIentific RESearch and Information Technology, 5, 2015.
[13] J.B. Barreau, T. Nicolas, G. Bruniaux, E. Petit, B. Petit, Y. Bernard, R. Gaugne, V. Gauranton, Ceramics fragments digitization by photogrammetry, reconstructions and applications, in: Proceedings of International Conference on Culturage Heritage, EuroMed, Lemossos, Cyprus, 2014 November 2014.
[14] M. Breuer, R.M. Czichon, M. Koch, M. Lehmann, D.P. Mielke, Photogrammetrische 3D-Dokumentation von Nassholzfunden aus Oymaagac Höyük/Nerik (Provinz Samsun /TR), Restaurierung und Archäologie (10) (2020) 47–62.
[15] R. Quattrini, R. Nespeca, L. Ruggeri, Digital photogrammetry for archaeological artefacts acquisition, in: Proceedings of IMEKO international conference on metrology for archaeology and Cultural Heritage, Lecce, Italy, 2017, pp. 643–648. October 23-25.
[16] P. Waldhäusl, C.L. Ogleby, 3×3 rules for simple photogrammetric documentation of architecture, Int. Arch. Photogramm. Remote Sens. 30 (1994) 426–429.
[17] TheoLt 2010 photography for photoplan3d: the 3×3 rules. Available at: http://www.theolt.com/web/photography-for-photoplan3d-the-3x3-rules/.
[18] J. Schöning, G. Heidemann, Evaluation of multi-view 3D reconstruction software, in: Proceedings of the International Conference on Computer Analysis of Images and Patterns, Valletta, Malta, 2015, pp. 450–461. 22–24 August.

[19] S.P. Singh, K. Jain, V.R. Mandla, Image based 3D city modeling: comparative study, Int. Arch. Photogramm. Remote Sens. Spat. Inf. Sci. 40 (2014) 537.
[20] L. Di Angelo, P. Di Stefano, Axis estimation of thin-walled axially symmetric solids, Pattern. Recognit. Lett. 106 (2018) 47–52.
[21] H. Pottmann, M. Peternell, B. Ravani, An introduction to line geometry with applications, Comput. Aid. Des. 31 (1999) 3–16.
[22] Y. Cao, D. Mumford, Geometric structure estimation of axially symmetric pots from small fragments, in: Proceedings of Signal Processing, Pattern Recognition, and Applications, IASTED International Conference, Crete, Greece, 2002 June 25 –28.
[23] A. Karasik, U. Smilansky, 3D scanning technology as a standard tool for pottery analysis: practice and theory, J. Archaeol. Sci. 35 (2008) 1148–1168.
[24] R. Halir, An automatic estimation of the axis of rotation of fragments of archaeological pottery: a multi-step model-based approach, in: Proceedings of the 7th International Conference in Central Europe on Computer Graphics, Visualization and Interactive Digital Media (WSCG99), Plzen, Czech Republic, West Bohemia, 1999 February 8-12.
[25] D. Han, H.S. Hahn, Axis estimation and grouping of rotationally symmetric object segments, Pattern. Recognit. 47 (2014) 296–312.
[26] D. Marquardt, An algorithm for least-squares estimation of nonlinear parameters, J. Appl. Math. 11 (1963) 31–441.
[27] H.F. Köhn, J.H. Lawrence, Hierarchical cluster analysis, Wiley StatsRef: Stat. Ref. Online (2014) 1–13.
[28] P.N. Tan, M. Steinbach, V. Kumar, Data mining cluster analysis: basic concepts and algorithms, Introduct. Data Min. 487 (2013) 533.
[29] T., Wu, L., Pan, J., Zhang, T., Wang, Z. Liu, D., Lin, Density-aware chamfer distance as a comprehensive metric for point cloud completion. arXiv preprint arXiv:2111.12702 (2021).
[30] A. Karasik, U. Smilansky, Computerized morphological classification of ceramics, J. Archaeol. Sci. 38 (10) (2011) 2644–2657.